Chapter 3

Franck-Condon blockade and giant Fano factors – Electronic avalanches

3.1 Introduction

The Fano factor F, defined as the ratio $S(\omega = 0)/2e\,|I|$ of the zero-frequency current noise and the classical Schottky result for Poissonian shot noise [95], contains information about the charge of the current-carrying particles, and about quantum correlations between them. Typically, the Pauli principle leads to suppressed Fano factors ($F < 1$) for fermionic carriers [96]. However, super-Poissonian noise has been discovered in systems with instabilities [96–98], and, very recently, with dynamical spin blockade [99]. In this chapter, we report surprisingly large Fano factors in transport through single molecules, which originate from the coupling of electronic and vibrational degrees of freedom, but are unrelated to instabilities.

We investigate the regime of *strong electron-phonon coupling* by current-voltage (IV) and noise calculations. It is found that strong electron-phonon coupling leads to a significant current suppression at low bias voltages, which we term *Franck-Condon blockade*. The striking transport properties of this regime are further elucidated by computing the current fluctuations. We find that systems with weak vibrational relaxation can exhibit *giant Fano factors* of the order of 10^2–10^3. This occurrence of giant Fano factors is due to avalanche-like transport of electrons interrupted by long times without charge transfer. These avalanches occur in a self-similar manner over a wide range of time scales, which is reflected in power-law behavior of the noise amplitude over many orders of magnitude in frequency and relaxation rate. The foundations of the FC blockade regimes and numerical results based on the rate-equations formalism are presented in Section 3.2.

In the subsequent Section 3.3 we establish an analytical description of self-similar avalanche transport. This allows us to study analytically the full counting statistics and noise spectrum of charge transport in this regime. The specifics of transport in the FC-blockade regime make the counting statistics strongly non-Gaussian. We support our findings for the counting statistics as well as for the frequency-dependent noise power by numerical simulations, finding excellent agreement.

3.2 Foundation of the Franck-Condon blockade and numerical results

3.2.1 Franck-Condon blockade

The strong dependence of the IVs on the electron-phonon coupling strength λ is shown in Fig. 3.1(a) for $\lambda = 1$ (intermediate coupling) and $\lambda = 4$ (strong coupling), as obtained from the rate-equation approach. We first consider the case of $\varepsilon_d = 0$, i.e. the molecular single-particle level and the lead Fermi energies are aligned at zero bias. Then, for $\lambda = 1$, the current increases sharply due to resonant tunneling when switching on a small bias voltage, and it exhibits the characteristic FC steps. In contrast, for $\lambda = 4$ the current is *significantly suppressed* at low bias voltages.

The current suppression originates from the behavior of the FC matrix elements determining the rates of phononic transitions $q_1 \to q_2$. Their dependence on the electron-phonon coupling strength can be understood in terms of the overlap of two displaced harmonic oscillator wave functions. The parameter λ determines the magnitude of this displacement in units of the oscillator length. For weak coupling, $\lambda \ll 1$, transitions mainly occur along the diagonal $q_1 \to q_1$. For intermediate coupling, $\lambda \approx 1$, the distribution of transition rates becomes wider, and transitions slightly off-diagonal are favored. For strong electron-phonon coupling, $\lambda \gg 1$, the distribution widens considerably and a gap of exponentially suppressed transitions between low-lying phonon states opens, see Fig. 3.1(b). It is interesting to note that these ingredients are also crucial in the context of phonon broadening of resonant-tunneling line shapes [41].

For temperatures $k_B T \ll \hbar\omega_0$, a tunneling event can increase the number of excited phonons by at most $\Delta q = \lfloor |eV| / 2\hbar\omega_0 \rfloor$ due to energy conservation.[1] Thus, for strong electron-phonon coupling and at low bias voltages, the system is trapped in a region of exponentially small transition rates. For equilibrated phonons ($\tau = 0$) this suppression dominates the IV until the bias voltage is high enough ($eV \sim \lambda^2 \hbar\omega_0$) to escape from the blockade regime by transitions from the vibrational ground state to highly excited phonon states. For unequilibrated phonons ($\tau = \infty$) the blockade is less rigorous, since a tunneling event can leave the molecule in an excited phonon state and subsequent tunneling events can increase this excitation even further.

There exist two experimental fingerprints of the FC blockade, which can be readily used to distinguish it from other low-bias current suppressions, such as off-resonance tunneling for $\varepsilon_d \neq 0$ and Coulomb blockade. In ungated devices, the succession of FC step heights yields a fingerprint of the origin of the blockade regime. For symmetric devices with strong phonon relaxation, the presence of FC blockade is reflected in increasing step heights when leaving the voltage range of current suppression. For asymmetric devices or weak phonon relaxation, this criterion does not hold for each single step but still gives a valid tendency for the step-height succession. (We point out that systems with strong electron-phonon coupling and weak relaxation can even exhibit NDR phenomena as indicated by negative values for dI/dV in Fig. 3.1(c) in red color.) When working with gated devices, a clear distinction can be achieved by measuring dI/dV as a function of both bias and gate voltage. Here, the FC blockade can be identified by an extended blockaded region in the eV–ε_d plane, whereas an $\varepsilon_d \neq 0$ suppression and Coulomb blockade can always be lifted by an appropriate adjustment

[1] Here, $\lfloor x \rfloor$ denotes the largest integer less than or equal to x.

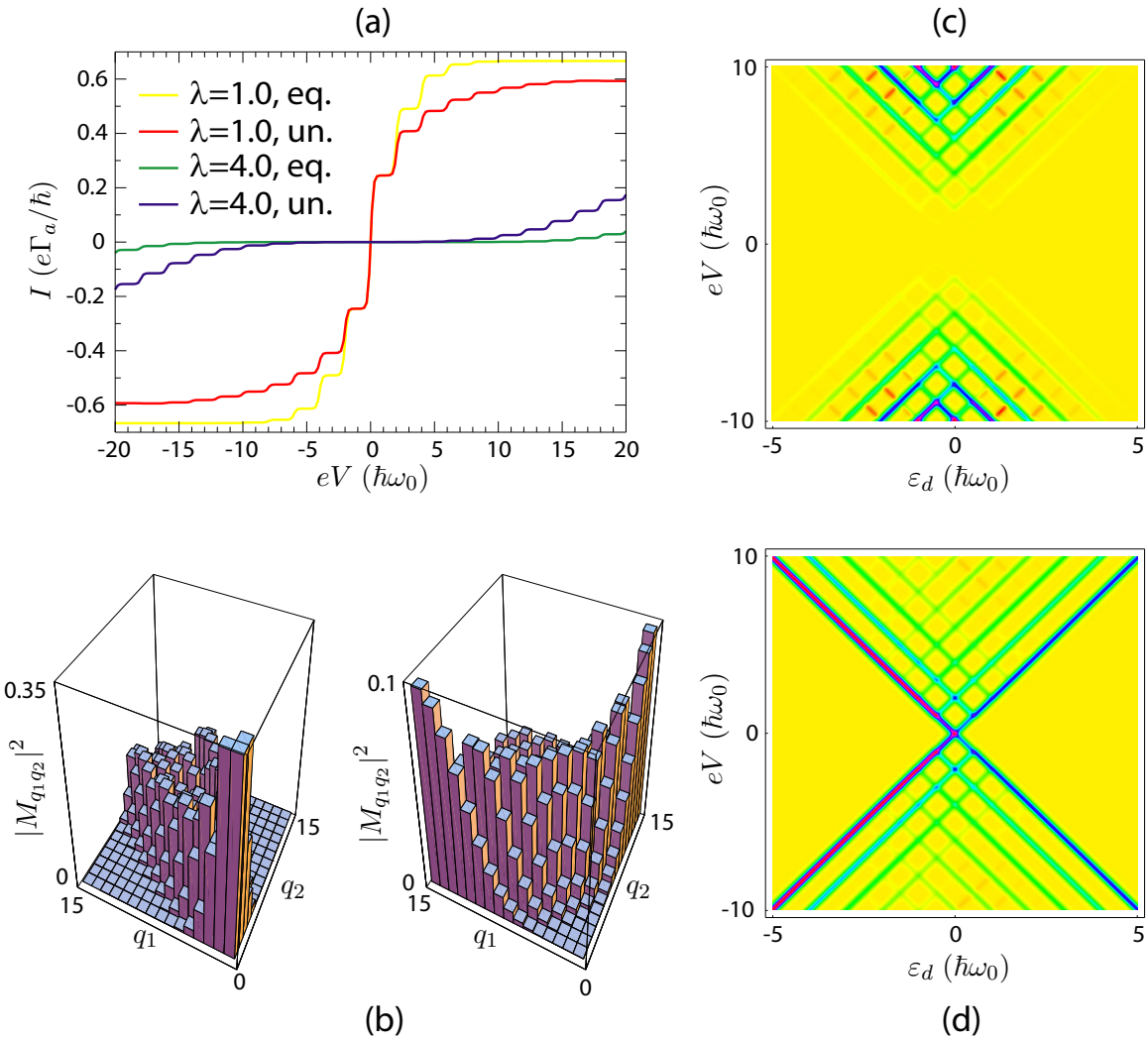

Figure 3.1: (a) Current-voltage characteristics for intermediate ($\lambda = 1$) and strong ($\lambda = 4$) electron-phonon coupling for $k_BT = 0.05\hbar\omega_0$ with (eq.) and without (un.) relaxation of phonons. We find that strong electron-phonon coupling leads to a significant current suppression at low bias voltages. This Franck-Condon blockade arises from the behavior of the Franck-Condon matrix elements for phonon transitions $q_1 \to q_2$. In (b), the square of the Franck-Condon matrix element is shown as a function of initial and final phonon states for $\lambda = 1$ (left) and $\lambda = 4$ (right). For strong electron-phonon coupling, transitions between low lying phonon states are exponentially suppressed. The corresponding current suppression cannot be lifted by a gate voltage, which may serve as a fingerprint of FC blockade. This is depicted in the plot of dI/dV in the V–V_g plane for unequilibrated phonons with $\lambda = 4$ (c). The case of intermediate coupling with $\lambda = 1$ (d) is shown for comparison.

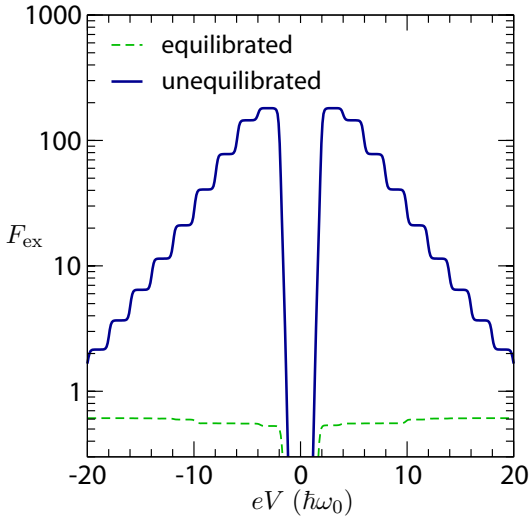

Figure 3.2: Zero-frequency (excess) Fano factor as a function of bias voltage with $\lambda = 4$ for $\varepsilon_d = 0$ and $k_BT = 0.05\hbar\omega_0$. Results are shown for equilibrated phonons ($\tau = 0$) and unequilibrated phonons ($\tau = \infty$). We find that the combined effect of strong electron-phonon coupling and weak phonon relaxation leads to giant Fano factors in the Franck-Condon blockade regime.

of the gate voltage, see Figs. 3.1(c),(d).

3.2.2 Giant Fano factors

The remarkable transport properties of the FC blockade regime are elucidated by computing the current fluctuations. We use Monte Carlo (MC) methods to simulate the explicit temporal dynamics of tunneling events, and rate equations combined with a Langevin approach [84] to calculate the current noise

$$S(\omega) = 2\int_{-\infty}^{\infty} d\tau\, e^{i\omega\tau}\left[\langle I(\tau+t)I(t)\rangle_t - \langle I(t)\rangle_t^2\right], \tag{3.1}$$

see Appendix D for further details. Here, we restrict our discussion to symmetric junctions so that, according to the Ramo-Shockley theorem [96], the current is given by $I(t) = [I_L(t) + I_R(t)]/2$. Typical results for strong and weak phonon relaxation are depicted in Fig. 3.2, where the zero-frequency Fano factor $F_{\rm ex}$ for the excess noise $S - S|_{V=0}$ is plotted as a function of bias voltage. For equilibrated phonons, $F_{\rm ex}$ is suppressed below 1 and except for weak step-like structures, it remains essentially constant in close vicinity of $F = 5/9$ expected for the phononless system with one spin-degenerate level and strong Coulomb blockade [100].

In contrast, for unequilibrated phonons with $\lambda = 4$ the Fano factor reaches values close to 200 as soon as the bias voltage is high enough for exciting the first phonon, and subsequently decreases stepwise at bias voltages corresponding to the opening of further phonon channels.[2] For bias voltages sufficient to lift the FC blockade, the Fano factor

[2]We note that even larger Fano factors of the order of 10^3 for $\lambda = 4$ occur for nonzero single-particle energy $\varepsilon_d \neq 0$. The origin of this off-resonance enhancement is explained in Section 3.3.5.

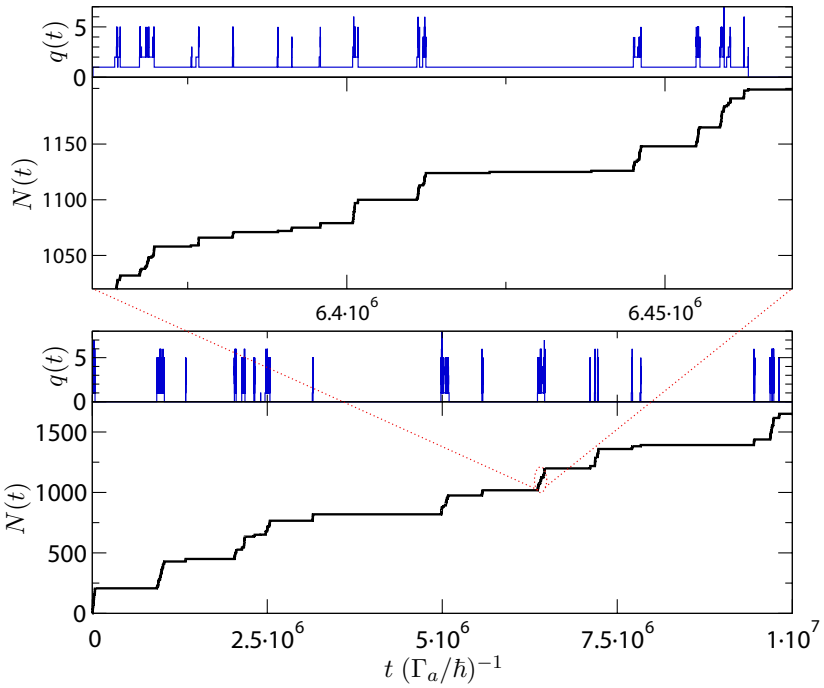

Figure 3.3: Number of transmitted electrons N and number of excited phonons q as functions of time, obtained by MC simulation for $T = 0.05\hbar\omega_0$, $eV = 3\hbar\omega_0$, $\varepsilon_d = 0$, $\tau = \infty$, and $\lambda = 4$. The upper plot shows a magnification of the marked region in the lower plot. The results show long periods of time without current flow when the system assumes the phononic ground state, and avalanche-like current flow accompanied by phonon excitations on much shorter time scales. Self-similarity of the curves is found when magnifying the avalanche phases.

returns to values of the order of 1.

3.2.3 Self-similar electron avalanches

The physics of the giant Fano factor originates from the combined effects of FC blockade and weak phonon relaxation, and can be understood by considering the time-dependent dynamics of the system. Results from a MC simulation of the tunneling events for $k_BT \ll \hbar\omega_0$ and strong electron-phonon coupling are shown in Fig. 3.3 (bottom), where the number of transmitted electrons N within the time interval $[0, t]$ and the number of excited phonons q are plotted as functions of time t. [A sketch of the principles of MC simulations for Markov processes is provided in Appendix F.] We find that for large periods of time the system assumes the phononic ground state $q = 0$ and the current vanishes (i.e. N is constant). These phases are interrupted by *avalanche-like increases* of N (accompanied by phonon excitations) on much shorter time scales. When magnifying the avalanche phases, we detect self-similarity of the curves $N(t)$ and $q(t)$, see Fig. 3.3 (top): Again, one observes long times with constant N, now associated with the first excited vibrational state $q = 1$, and short avalanche phases.

The extended phases without charge transfer are due to the suppressed transition rates

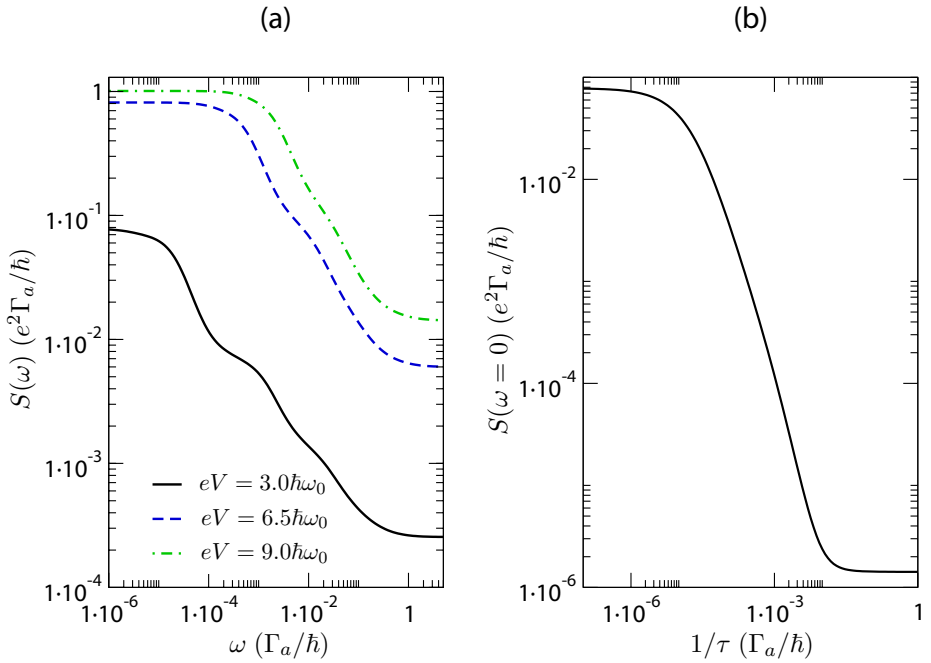

Figure 3.4: Noise power in the Franck-Condon blockade regime as a function of (a) frequency, and (b) phonon relaxation rate for $\varepsilon_d = 0$, $\lambda = 4$, and $k_B T = 0.05\hbar\omega_0$. In (a) the total current noise is plotted for unequilibrated phonons. In (b) the zero-frequency noise is plotted for the bias voltage $eV = 3\hbar\omega_0$. We find (approximate) power-law behavior $S(\omega) \sim \omega^{-\alpha}$ and $S(0) \sim \tau^{1/\alpha}$ with $\alpha \approx 1/2$, arising from the self-similar avalanches over a wide range of time scales.

for low-lying phonon states in the FC blockade regime. Typically, the system spends a long time in the phononic ground state before a transition takes place. Starting from $q = 0$ and for voltages $2\hbar\omega_0 < |eV| < 4\hbar\omega_0$, where the Fano factor is maximal, energy conservation only allows the phonon transitions $0 \to 0$ and $0 \to 1$. Since the rates for phonon transitions $0 \to q_2$ roughly grow exponentially with q_2, it is favorable to increase the phonon number whenever an electronic transition occurs. Thus, as soon as the system succeeds in leaving the phononic ground state and if phonon relaxation is weak, subsequent transitions tend to increase the phonon number even further, while the transition rates increase roughly exponentially. Then, after having left the regime of suppressed transition rates, the system can exhibit an avalanche of tunneling events, until an accidental transition to the phononic ground state induces another long period without charge transfer, and the cycle repeats. Effectively, this leads to electron bunching, and the Fano factor can be estimated by the typical number of electrons transmitted during an avalanche, see Fig. 3.3.

The remarkable self-similarity of avalanche phases due to the exponential stretching of transition rates is reflected in the relaxation-rate dependence of the Fano factor and the noise power spectrum, depicted in Fig. 3.4. In both cases, we find approximate power-law behavior, $S \sim \omega^{-\alpha}$ and $S \sim \tau^{1/\alpha}$ with $\alpha \approx 1/2$, over many orders of magnitude in relaxation rate and frequency, respectively. (In some cases with $\lambda = 4$ and $\varepsilon_d \neq 0$, we found this power-law behavior to extend over 6 orders of magnitude in ω and $1/\tau$.) The boundaries of the power-law scaling in the frequency domain are connected to the maximum

available transition rate, and to the "smallest" transition rate describing the escape from the phononic ground state. The weak oscillatory deviations from a pure power law arise from the discreteness of the variable q.

3.3 Analytical theory of avalanche transport

We now turn to the development of an analytical theory of the regime of avalanche transport. Our starting point is the time dependence of the current in the strong-coupling regime, which can be presented as

$$I(t) = f_1^{(0)}(t - t_1) + f_2^{(0)}(t - t_1 - t_2) + \ldots, \tag{3.2}$$

where t_i are the time intervals between avalanches (quiet periods). These intervals are much longer than the typical duration $\tau^{(0)}$ of an avalanche, which occurs during the sparse periods when the vibrations are excited. The random function $f_i^{(0)}(t)$ (which is nonzero only for times $|t| \lesssim \tau^{(0)}$) describes the passage of a *large number* $\int dt\, f_i^{(0)}(t) = N_i \gg 1$ of electrons through the molecule during the ith avalanche. Moreover, the numerical study of the avalanches (Section 3.2) revealed their self-similar hierarchical structure, see Fig. 3.5. Quantitatively, this structure manifests itself in the fact that, during the time of an avalanche $\sim \tau^{(0)}$, each function $f_i^{(0)}$ itself takes the form of Eq. (3.2), with $f_i^{(0)}$ replaced by random functions $f_i^{(1)}$, which describe *generation–1 avalanches* interrupted by quiet periods.[3] Again, these quiet periods are much longer than the characteristic time scale $\tau^{(1)}$ of the functions $f_i^{(1)}$. For times shorter than $\tau^{(1)}$, the functions $f_i^{(1)}$ have the form of Eq. (3.2) with corresponding generation–2 avalanches, $f_i^{(2)}$, having even shorter time-scale, $\tau^{(2)}$, and so on.[4] Numerical results supporting this scenario are shown in Fig. 3.5.

The above discussion implies that the statistical properties of charge transport through a molecule in the regime of strong electron-phonon coupling and through a conventional nanostructure are drastically different. For a nanostructure, all $f_i^{(0)}$ are δ functions, so that $N_i = 1$. Hence, the distribution function $P_t(Q)$ of the net transmitted charge Q during time t (full counting statistics [101]) is completely encoded in the distribution of the *waiting times* t_i for single-electron transitions. This distribution reflects the details of the transport mechanism, and might be quite nontrivial [96]. Nevertheless, with all t_i being of the same order, the full counting statistics differs only weakly from a Gaussian distribution. Small deviations are caused by correlations [102, 103], interactions [104], or the influence of the environment [105], and have been extensively studied theoretically.

By contrast, the counting statistics of avalanche-type transport is *insensitive* to the details of the passage of a single electron through the molecule, since the number of electrons involved in each avalanche is large. Instead, the counting statistics is governed *exclusively* by the transition rates between different vibrational states. These rates have a simple structure in the limit of strong coupling which allows us to develop a complete analytical theory for the regime of avalanche-type transport. In particular, we demonstrate in this section that

[3] A generation–q avalanche ($q = 0, 1, \ldots$) is characterized by waiting periods associated with the occupation of the vibrational state q.

[4] The hierarchy breaks off once the transferred charge per avalanche is of the order of unity.

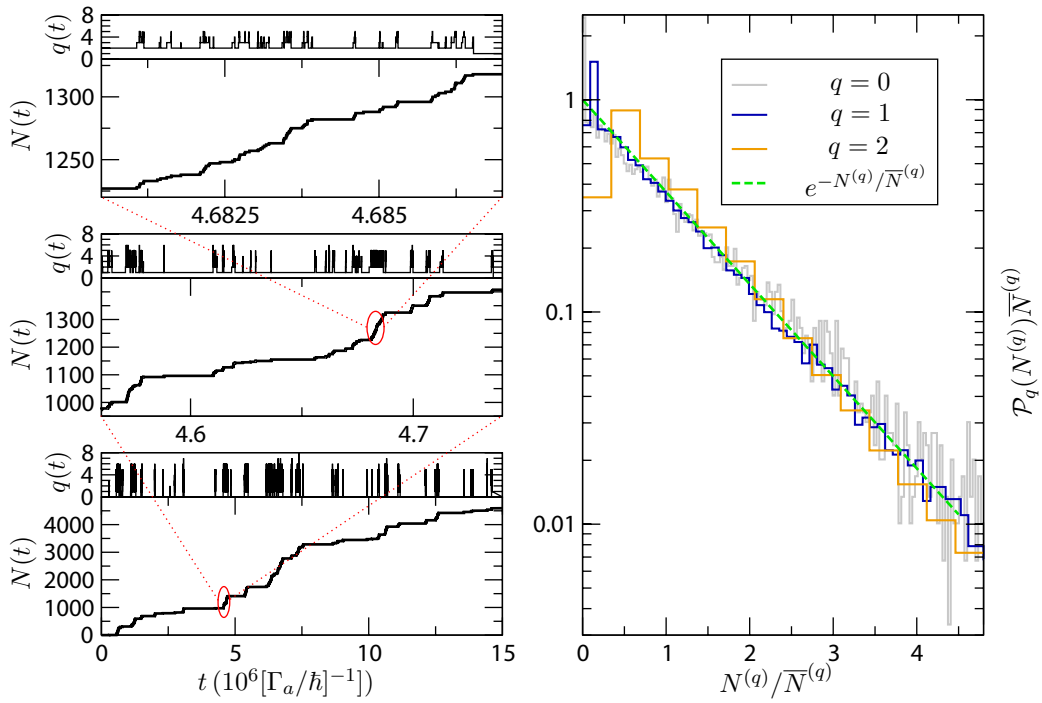

Figure 3.5: Hierarchical character of transport. Left: Three generations of self-similar MC plots for $\lambda = 4$ and $eV = 3\hbar\omega_0$, showing the net-transferred charge N and phonon state q as functions of time. (ω_0: phonon frequency; ρ: density of states of the leads; Γ_a: tunneling-induced level width). Right: Comparison of the fixed-point distribution for the transferred charge per generation–q avalanche to numerical simulations for $q = 0, 1, 2$ (mean values $\overline{N}^{(0)} = 91.2$, $\overline{N}^{(1)} = 11.1$, and $\overline{N}^{(2)} = 2.9$).

the full counting statistics $P_t(Q)$ is given by a concise analytical expression, which is strongly skewed at "short" times (i.e. of the order of the zero-order quiet period) and evolves into a Gaussian only for very large t. Along with the counting statistics, we also study analytically how the hierarchy of avalanches manifests itself in the frequency dependence of the noise power $S(\omega)$. Our analytical results are in excellent agreement with numerical Monte-Carlo simulations. For easier reference, the definitions of the most important quantities used in the following subsections are listed in Table 3.1. Some calculational details are deferred to Appendix E to keep the main line of thought uninterrupted.

3.3.1 Full counting statistics

Since different generation–0 avalanches are statistically independent, it is easy to derive a relation between the counting statistics $P_t(Q)$ of the *net charge* Q and the conventional counting statistics $\varphi_t(n)$ [101] of the *number* of generation–0 avalanches n during the time interval t. Indeed, using the definition $P_t(Q) = \langle \delta(Q - \sum_{j=1}^{n} N_j) \rangle_{N_j,n}$, and a Fourier representation of the right-hand side, one obtains

$$P_t(Q) = \int \frac{d\alpha}{2\pi} e^{i\alpha Q} \sum_n \left[\tilde{\mathcal{P}}_0(\alpha)\right]^n \varphi_t(n), \tag{3.3}$$

$P_t(Q)$	full counting statistics (probability that the net charge Q is transferred within the time interval t
$\varphi_t(n)$	counting statistics for avalanches (probability that n generation–0 avalanches occur during the time interval t)
$\mathcal{P}_q(N)$	distribution function for the number N of electrons per generation–q avalanche
$p_q(n)$	distribution function for the number n of generation–$(q+1)$ avalanches in a generation–q avalanche
$W(t)$	distribution of waiting times between generation–0 avalanches
$\overline{N}^{(q)}$	mean number of electrons per generation–q avalanche
$\overline{n}_t$	mean number of generation–0 avalanches during the time interval t
$\overline{n}_q$	mean number of generation–$(q+1)$ avalanches in a generation–q avalanche
$\tau^{(q)}$	mean duration of a generation–q avalanche
$t^{(q)}$	average waiting time $\langle t_i \rangle$ between avalanches at level q of the hierarchy

Table 3.1: List of definitions for the analytical treatment of avalanche transport.

where $\tilde{\mathcal{P}}_0(\alpha) = \langle \exp(-i\alpha N_j) \rangle_{N_j}$ denotes the Fourier transform of the distribution function $\mathcal{P}_0(N)$ of the total charge passing per generation–0 avalanche. The durations of the quiet periods are exponentially distributed, which results in Poisson statistics for the counting statistics of avalanches,

$$\varphi_t(n) = \frac{\exp(-\overline{n}_t)[\overline{n}_t]^n}{n!}. \tag{3.4}$$

Here, $\overline{n}_t$ denotes the average number of generation–0 avalanches within time t. Substituting this form into Eq. (3.3) and performing the summation over n yields an expression for the counting statistics similar to the Holtsmark distribution [106],

$$P_t(Q) = \int \frac{d\alpha}{2\pi} \exp\left\{ i\alpha Q + \overline{n}_t \left[\tilde{\mathcal{P}}_0(\alpha) - 1 \right] \right\}. \tag{3.5}$$

Thus, the problem of the counting statistics is reduced to finding the distribution $\mathcal{P}_0(N)$. Two facts allow us to find $\mathcal{P}_0(N)$, namely

(i) the self-similar structure of avalanches, and

(ii) the large number n_q of generation–$(q+1)$ avalanches within a given generation–q avalanche.

Our basic observation is that we can derive a recursion relation, relating the distribution functions $\mathcal{P}_q(N)$ and $\mathcal{P}_{q+1}(N)$ of the total passing charge ($N^{(q)}$ and $N^{(q+1)}$, respectively) per avalanche for subsequent generations. This recursion follows from the obvious facts that $N^{(q)} = \sum_{j=1}^{n_q} N_j^{(q+1)}$ and that different avalanches of a given generation are statistically independent. By analogy with the derivation of Eq. (3.3), we thus obtain

$$\mathcal{P}_q(N) = \int \frac{d\alpha}{2\pi} e^{i\alpha N} \sum_n \left[\tilde{\mathcal{P}}_{q+1}(\alpha) \right]^n p_q(n), \tag{3.6}$$

where $p_q(n)$ denotes the distribution function of n_q. To proceed further, one has to specify the form of the distribution $p_q(n)$. This distribution is governed by the *microscopic* characteristics of the Franck-Condon transitions. We demonstrate below that $p_q(n) =$

$(1/\overline{n}_q)\exp(-n/\overline{n}_q)$.[5] Upon substituting this form into Eq. (3.6), the summation over n on the right-hand side can be easily performed and we obtain, after a Fourier transform of both sides,

$$\tilde{\mathcal{P}}_q(\alpha) = \frac{1}{1-\overline{n}_q \ln[\tilde{\mathcal{P}}_{q+1}(\alpha)]}. \tag{3.7}$$

The distribution $\mathcal{P}_q$ can now be obtained from this equation by writing its general solution as $\tilde{\mathcal{P}}_q(\alpha) = [1 + i\alpha\overline{N}^{(q)} + c_q(\alpha\overline{N}^{(q)})^2 + \ldots]^{-1}$. Inserting this into Eq. (3.7), we find that the numerical coefficients c_q flow to zero with q by virtue of the small parameter $1/\overline{n}_q$, see Appendix E for further details. Thus, the solution $\tilde{\mathcal{P}}_q(\alpha) = [1 + i\alpha\overline{N}^{(q)}]^{-1}$ with Fourier transform

$$\mathcal{P}_q(N) = \theta(N)\exp\left[-N/\overline{N}^{(q)}\right]/\overline{N}^{(q)} \tag{3.8}$$

can be viewed as a fixed point of the recursion equation Eq. (3.6) and since $\overline{N}^{(q)} = \overline{n}_q\overline{N}^{(q+1)}$, self-similarity is obeyed asymptotically. The existence of this fixed-point solution is a consequence of remark (i) which implies that up to rescalings, the distribution functions $\mathcal{P}_q(N)$ have the same functional form for *all* q. Fig. 3.5 numerically confirms this result for three different generations.

With $\mathcal{P}_q(N)$ established, we obtain the counting statistics by substituting $\tilde{\mathcal{P}}_0(\alpha) = (1 + i\alpha\overline{N}^{(0)})^{-1}$ into Eq. (3.3) and performing the integral and summation, see Appendix E. This yields

$$P_t(Q) = e^{-\overline{n}_t}\delta(Q) + e^{-\frac{Q}{\overline{N}^{(0)}}-\overline{n}_t}\sqrt{\frac{\overline{n}_t}{\overline{N}^{(0)}Q}}\,\mathrm{I}_1\left(\sqrt{\frac{4\overline{n}_tQ}{\overline{N}^{(0)}}}\right). \tag{3.9}$$

Here, $\mathrm{I}_1(z)$ denotes a modified Bessel function. Eq. (3.9) is our central result. It is nicely confirmed by MC simulations as shown in Fig. 3.6, and describes the evolution of the counting statistics between the following two transparent limits.

Short times

For short times, $\overline{n}_t = t/\langle t_i\rangle \ll 1$, we use the expansion $\mathrm{I}_1(z) \approx z/2$ for $z \ll 1$ and obtain from Eq. (3.9)

$$P_t(Q) \simeq e^{-\overline{n}_t}\left[\delta(Q) + (\overline{n}_t/\overline{N}^{(0)})e^{-Q/\overline{N}^{(0)}}\right]. \tag{3.10}$$

Typically only a few electrons are transmitted through the molecule. The long tail described by the second term in Eq. (3.10) arises from realizations where an avalanche occurs within the time t and reflects the spread of charge within a single avalanche.

Long times

For long times, $\overline{n}_t \gg 1$, we substitute the large-z asymptote of $\mathrm{I}_1(z)$ into Eq. (3.9). Then, it is easy to see that the second term has a sharp maximum centered at $Q = \overline{n}_t\overline{N}^{(0)}$, which

[5] Here, we exploit that the average number of subavalanches is large, $\overline{n}_q \gg 1$. This allows us to treat n as a continuous variable.

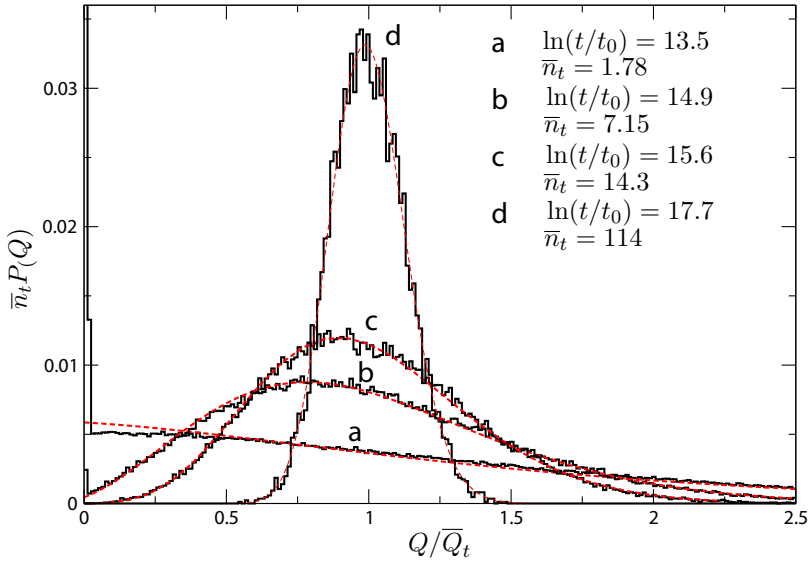

Figure 3.6: Evolution of full counting statistics $P_t(Q)$ for four different time intervals t with $\lambda = 4.0$ and $eV = 3\hbar\omega_0$. The MC data (solid lines) are in excellent agreement with the analytical full counting statistics, Eq. (3.9), (dashed lines), with $\overline{N}^{(0)} = 91.2$ and $\overline{n}_t = 2.4 \cdot 10^{-6} t/t_0$ (no fit), as well as $t_0 = (\Gamma_a/\hbar)^{-1}$.

is the average charge passed through the molecule after a large number of avalanches. Expansion of the exponent around the maximum yields the Gaussian

$$P_t(Q) \simeq (\sqrt{2\pi}\sigma_Q)^{-1} \exp\left[-\left(Q - \overline{n}_t \overline{N}^{(0)}\right)^2 / 2\sigma_Q^2\right] \tag{3.11}$$

with a width $\sigma_Q = (2\overline{n}_t)^{1/2}\, \overline{N}^{(0)}$. This width is *twice* the width expected from the fluctuations of the waiting times. This enhanced broadening is due to fluctuations of the charge passed per avalanche. These additional fluctuations also manifest themselves in the noise characteristics of transport as analyzed below.

3.3.2 Microscopic derivation of $p_q(n)$

The distribution $p_q(n)$ for the number n of generation–$(q+1)$ avalanches in a generation–q avalanche can be derived in the following way. We first generalize the distribution $\varphi_t(n)$ to higher generations, i.e. we define $\varphi_t^{(q)}(n)$ as the distribution of the number n of generation–q avalanches within a generation–$(q-1)$ avalanche which occur during the time interval t. The self-similarity of avalanches implies that these higher-generation distributions must obey Poisson statistics as well.

Now, the distribution $p_q(n)$ is obtained by averaging the Poisson distribution of n for a *given* avalanche duration over the distribution of *durations* $\tau_i^{(q)}$, i.e.

$$p_q(n) = \left\langle \frac{\exp\left[-\tau_i^{(q)} w_q\right] \left(\tau_i^{(q)} w_q\right)^n}{n!} \right\rangle_{\tau_i^{(q)}}. \tag{3.12}$$

Here, w_q denotes the average rate for starting a generation–$(q+1)$ avalanche from the level q. On microscopic grounds, the distribution of durations is a simple exponential distribution, which immediately transforms into $p_q(n) = (1/\overline{n}_q)\exp(-n/\overline{n}_q)$ since $\overline{n}_q$ is large.

To see that the duration distribution is exponential, we note that the mean duration $\tau^{(q)}$ of a generation–q avalanche is determined by the waiting times in the vibrational state $q+1$ since the durations of intermittent higher-generation avalanches can be neglected. Two processes terminate a generation–q avalanche: a direct transition from $q+1$ to q or a transition back to q during a generation–$(q+1)$ avalanche. Denoting the total rate for both processes by Γ_q, we obtain an exponential distribution of durations, $\Gamma_q \exp(-\Gamma_q \tau^{(q)})$.

3.3.3 Noise spectrum $S(\omega)$ of avalanche-type transport

We first derive a general expression for $S(\omega)$ assuming arbitrary distributions $\mathcal{P}_0(N)$ of the avalanche magnitudes and $W(t)$ of the waiting times. For frequencies smaller than $1/\tau^{(0)}$, we have $f_i^{(0)}(t) \simeq N_i\delta(t)$ in Eq. (3.2). Using Fourier representations of the δ functions and averaging over the t_i and N_i, the average current becomes

$$\langle I(t)\rangle = \langle N_i\rangle \int \frac{d\alpha}{2\pi} e^{i\alpha t} \frac{\tilde{W}(\alpha)}{1-\tilde{W}(\alpha)}, \tag{3.13}$$

where $\tilde{W}(\alpha) = \langle \exp(-i\alpha t_i)\rangle_{t_i}$ denotes the Fourier transform of $W(t)$. In the long-time limit, only small values of α contribute to the integral in Eq. (3.13) so that we can use the expansion $\tilde{W}(\alpha) = 1 - i\alpha\langle t_i\rangle - (1/2)\alpha^2\langle t_i^2\rangle + \ldots$ Inserting this into Eq. (3.13), keeping only the leading order in α and performing the contour integration over α, we recover the obvious result $\langle I(t)\rangle = \langle N_i\rangle/\langle t_i\rangle$. [See Appendix E for details.] Similarly, we express the current-current correlator as

$$\begin{aligned}
&\langle I(t_1)I(t_2)\rangle \\
&= \int \frac{d\alpha}{2\pi}\frac{d\beta}{2\pi} e^{-i\alpha t_1 - i\beta t_2} \left\langle [N_1 e^{i\alpha t_1} + N_2 e^{i\alpha(t_1+t_2)} + \ldots][N_1 e^{i\beta t_1} + N_2 e^{i\beta(t_1+t_2)} + \ldots]\right\rangle \\
&= \int \frac{d\alpha}{2\pi}\frac{d\beta}{2\pi} e^{-i\alpha t_1 - i\beta t_2} \left[\frac{\langle N_i\rangle^2 \tilde{W}(\alpha+\beta)}{1-\tilde{W}(\alpha+\beta)} \left(\frac{1}{1-\tilde{W}(\alpha)} + \frac{1}{1-\tilde{W}(\beta)} - 1 \right) \right. \\
&\qquad \left. + \frac{(\langle N_i^2\rangle - \langle N_i\rangle^2)\tilde{W}(\alpha+\beta)}{1-\tilde{W}(\alpha+\beta)} \right].
\end{aligned} \tag{3.14}$$

The last equality follows upon term-by-term averaging and resummation of the series. To access the limit of long times $t = (t_1+t_2)/2$, we introduce $\omega = (\alpha-\beta)/2$ and $\Omega = \alpha+\beta$. Then, the exponent in the integrand in Eq. (3.14) assumes the form $\exp(i\omega\tau - i\Omega t)$ with $\tau = t_2 - t_1$. The limit $t \to \infty$ can now be taken in analogy with the derivation of $\langle I(t)\rangle$ above. The integrand can be directly identified with the noise spectrum $S(\omega)$, so that

$$S(\omega) = \frac{2}{\langle t_i\rangle}\left\{ \langle N_i\rangle^2 \left[\frac{1}{1-\tilde{W}(\omega)} + \frac{1}{1-\tilde{W}(-\omega)} - 1 \right] + (\langle N_i^2\rangle - \langle N_i\rangle^2) \right\}. \tag{3.15}$$

Taking the zero-frequency limit requires one to keep terms of order ω^2 in the expansion of $\tilde{W}(\pm\omega)$. In this way, the Fano factor $F = S(\omega=0)/2e\langle I\rangle$ becomes

$$F = \langle N_i\rangle \frac{\langle t_i^2\rangle - \langle t_i\rangle^2}{\langle t_i\rangle^2} + \frac{\langle N_i^2\rangle - \langle N_i\rangle^2}{\langle N_i\rangle}. \tag{3.16}$$

This equation allows for a transparent interpretation: Noise originates from two sources, namely the fluctuations in the intervals between avalanches and the fluctuations in the transmitted charge per avalanche. In the conventional situation where $N_i = 1$ for all i, the Fano factor is given by the fluctuations of the waiting times t_i for a transition in which an electron passes either directly or sequentially from the left to the right lead. For example, for transport through a symmetric junction in the Coulomb-blockade regime, one immediately recovers $F = 5/9$ [100] when taking into account that the rates of entering and leaving the dot are related as 2:1 due to spin. For the specific distributions adopted in our model, both terms in Eq. (3.16) contribute equally, and the Fano factor reduces to $F = 2\overline{N}^{(0)}$, which, in agreement with Eq. (3.11), is twice the value expected for a fixed magnitude of avalanches. This is confirmed by numerical results.

For frequencies larger than $1/\tau^{(0)}$, the "fine structure" of the avalanches described by the functions $f_i^{(0)}$ in Eq. (3.2) must be taken into account. This fine structure can be incorporated into the noise spectrum Eq. (3.15) by replacing

$$\langle N_i\rangle^2 \quad \to \quad \langle\tilde{f}(\alpha)\rangle\langle\tilde{f}(\beta)\rangle, \tag{3.17}$$

$$\langle N_i^2\rangle \quad \to \quad \langle\tilde{f}(\alpha)\tilde{f}(\beta)\rangle, \tag{3.18}$$

where $\tilde{f}(\alpha)$ denotes the Fourier transform. Explicitly employing the exponential distribution of the waiting times, we find the remarkable simplification $[1-\tilde{W}(\omega)]^{-1}+[1-\tilde{W}(-\omega)]^{-1}-1 = 1$. In this way, we obtain

$$S(\omega) = \frac{2}{\langle t_i\rangle}\langle\tilde{f}(\omega)\tilde{f}(-\omega)\rangle. \tag{3.19}$$

For frequencies of the order of $\omega \simeq 1/t^{(0)}$ (where $t^{(q)}$ denotes the average waiting time $\langle t_i\rangle$ at level q of the hierarchy), we can ignore the fine structure of the avalanche and replace $\tilde{f}(\omega) = N_i^{(0)}$. Thus, we find

$$S(\omega) = \frac{2\langle[N_i^{(0)}]^2\rangle}{t^{(0)}}. \tag{3.20}$$

At higher frequencies $\omega \simeq 1/t^{(1)}$, the function $f(t)$ is resolved into avalanches of generation $q = 1$. Then, we can write

$$\langle\tilde{f}(\omega)\tilde{f}(-\omega)\rangle = \int dt \int d\tau\, e^{i\omega\tau}\langle f(t+\tau/2)f(t-\tau/2)\rangle. \tag{3.21}$$

Up to the integral over t, this expression is analogous to $S(\omega)$ itself, with generation–0 quantities replaced by corresponding $q = 1$ quantities. For the frequencies of interest, we therefore find

$$S(\omega) = \frac{2}{t^{(0)}}\frac{\tau^{(0)}\langle[N_i^{(1)}]^2\rangle}{t^{(1)}}. \tag{3.22}$$

Using the obvious relations $\tau^{(0)} = t^{(1)}\overline{n}_0$ and $\overline{N}^{(0)} = \overline{n}_0\overline{N}^{(1)}$ and generalizing to arbitrary q, we conclude that

$$S_{q+1} = \frac{\overline{N}^{(q+1)}}{\overline{N}^{(q)}}S_q. \tag{3.23}$$

Here, we define $S_q = S(\omega \simeq 1/t^{(q)})$ so that Eq. (3.23) provides a rule for extending the noise spectrum to progressively higher frequencies.

The essential *microscopic* inputs are the ratios $t^{(q+1)}/t^{(q)}$ and $\overline{N}^{(q+1)}/\overline{N}^{(q)}$. Both ratios are determined by overlaps of displaced vibrational wavefunctions. The rate $1/t^{(q)}$ is dominated by the transition $q \to q+1$. Thus, it involves the overlap of *neighboring* harmonic oscillator states. By contrast, $\overline{N}^{(q)}$ is inversely proportional to the transition rate from a highly excited phonon level to the qth vibrational level. The difference between these two rates is thus that the first involves four wavefunctions with index of order q, while the second involves only two. As a result, we can immediately establish from a quasiclassical evaluation of the matrix elements that $t^{(q)}/(\overline{N}^{(q)})^2$ is essentially independent of q. With this input, we conclude that $S(\omega) \sim \omega^{-\alpha}$ with exponent $\alpha = 1/2$. Since the noise power does not depend sensitively on ω in finite intervals around $1/t^{(q)}$, this power law should be superimposed with steplike features in $S(\omega)$. These conclusions agree with numerical simulations over several orders of magnitude in frequency.

3.3.4 The role of vibrational relaxation

Finally, we remark that direct vibrational relaxation (with rate $\gamma_{\rm rel}$), neglected so far, only gradually suppresses avalanche-type transport. Indeed, the numerical results presented in Section 3.2 revealed a power-law scaling of the zero-frequency noise, $S(0) \sim 1/\gamma_{\rm rel}^2$, over a wide range of relaxation times. This relation can easily be justified on the basis of our previous analytical result $S(0) = 4e^2[\overline{N}^{(0)}]^2/t^{(0)}$. As confirmed by numerical MC data, the number of electrons transferred in a generation–0 avalanche is expected to scale linearly with the avalanche duration. This implies the relation $\overline{N}^{(0)} \sim \tau^{(0)}$. Vibrational relaxation adds an additional channel for terminating an avalanche, thus increasing the effective termination rate according to

$$\Gamma_e = \Gamma_0 + \gamma_{\rm rel}. \tag{3.24}$$

Here, we have defined $\Gamma_0 = 1/\tau^{(0)}$. Thus, the effective avalanche duration is shortened due to relaxation, also diminishing the average electron number $\overline{N}^{(0)}$,

$$\overline{N}^{(0)} \sim \tau_e = 1/\Gamma_e = \frac{1}{\Gamma_0 + \gamma_{\rm rel}}. \tag{3.25}$$

As soon as relaxation is the dominant limiting process, $\gamma_{\rm rel} \gg \Gamma_0$, we recover the observed power-law behavior $S(0) \sim 1/\gamma_{\rm rel}^2$.

3.3.5 Fano factor enhancement for nonzero ε_d

So far, we have mainly focused on the case of vanishing single-particle ε_d. Interestingly, as briefly mentioned in Section 3.2, the situation $\varepsilon_d \neq 0$ may cause a further increase of Fano factors as compared to the $\varepsilon_d = 0$ configuration, see Fig. 3.7. Especially large Fano factors are observed for low biases above the threshold $eV > \hbar\omega_0$ whenever the electronic level ε_d is roughly aligned with the Fermi energy of the right or left lead.

At first view, the resulting Fano factor enhancement is surprising since the mean number of electrons per avalanche is *decreased* for such a level configuration. For an understanding of this decrease, consider the case of level alignment with the left Fermi energy.

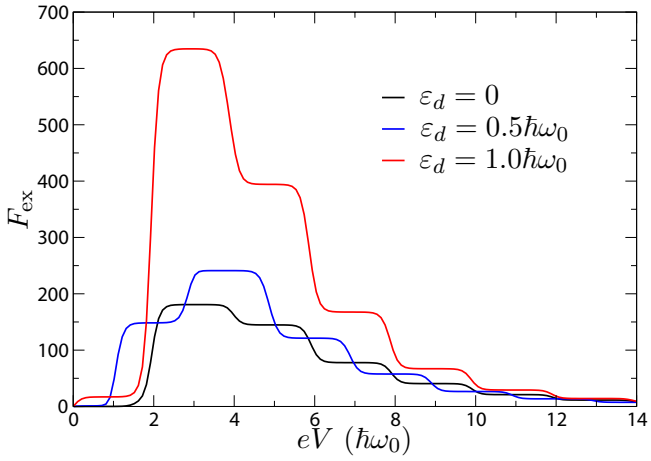

Figure 3.7: Excess noise Fano factor as a function of bias voltage for strong electron-phonon coupling ($\lambda = 4.0$) and different gate-voltages ε_d. Remarkably, the Fano factor is even further increased for nonzero ε_d, which is explained by the drastic enhancement of waiting-time fluctuations.

Then, phonon excitations can only occur through tunneling in the right junction. Events in the junction L can only decrease the phonon state (or leave it unchanged). Thus, every second tunneling event will inhibit phonon excitations. With avalanches benefitting from the possibility of reaching highly excited phonon states, the mean number of electrons per avalanche is reduced as compared to the case where the level is centered between the two Fermi levels. This decrease in $\langle N_i \rangle$ is confirmed by Monte-Carlo simulations.

The somewhat counterintuitive result that the Fano factor nevertheless becomes *larger* can be traced back to the significantly enhanced fluctuations in waiting times t_i, which directly contribute to the Fano factor, see Eq. (3.16). In the following, we explain this enhancement of waiting-time fluctuations. Any generation–0 avalanche may terminate either in the charge state $n = 0$ or $n = 1$, and the corresponding probabilities are denoted p_0 and p_1. After the avalanche termination, the system undergoes a waiting period t_i. The crucial point is that for level alignment with one Fermi energy, this waiting time strongly depends on the charge state n. Starting in the state $n = 0$, transitions in the left junction do not allow phonon excitations. By contrast, for the initial state $n = 1$ and transitions across the right junction, the excitation of phonons is favored (due to the increase of FC matrix elements towards highly excited vibrational states). Accordingly, the relevant two rates after avalanche termination are dramatically different, $W_{00}^{01} \ll W_{01}^{10}$, and the waiting times in the two cases will differ accordingly,

$$\langle t_i^{(n=0)} \rangle = (W_{00}^{01})^{-1} \gg \langle t_i^{(n=1)} \rangle = (W_{01}^{10})^{-1}. \tag{3.26}$$

Consequently, the probability distribution of waiting times is not given by a single exponential anymore, but is well approximated by

$$p(t_i) = p_0 W_{00}^{01} \exp[-W_{00}^{01} t_i] + p_1 W_{01}^{10} \exp[-W_{01}^{10} t_i]. \tag{3.27}$$

While the $\varepsilon_d = 0$ case with a simple exponential distribution results in $\left(\langle t_i^2 \rangle - \langle t_i \rangle^2\right) / \langle t_i \rangle^2 =$

1, we now find

$$\frac{\langle t_i^2\rangle - \langle t_i\rangle^2}{\langle t_i\rangle^2} \approx \frac{2-p_0}{p_0}, \tag{3.28}$$

valid for $p_0 \gg W_{00}^{01}/W_{01}^{10}$. By Monte-Carlo simulations we confirm that p_0 satisfies $1 > p_0 \gg W_{00}^{01}/W_{01}^{10}$ for realistic parameters. Therefore, Eq. (3.28) explains the off-resonance enhancement of Fano factors by the increase of waiting-time fluctuations.

3.4 Conclusions

Vibrational degrees of freedom can play an important role in transport through single molecules, and lead to transport properties very different from those of conventional semiconductor or metal nanostructures. In particular, we have shown that FC physics, which is *characteristic of molecules*, leads to a low-bias current suppression (FC blockade) and giant Fano factors of the order of 10^2–10^3 in single-molecule devices with strong electron-phonon coupling and weak phonon relaxation. The Fano factor enhancement has been explained by avalanche-like transport of electrons. The self-similar occurrence of such avalanches over a wide range of time scales is reflected in approximate power-law behavior of the noise as a function of frequency and relaxation rate.

Our complete analytical description for the full-counting statistics and the frequency-dependent noise power of self-similar avalanche-type transport was made possible by the fact that current flow is essentially unidirectional. We emphasize that our arguments are quite

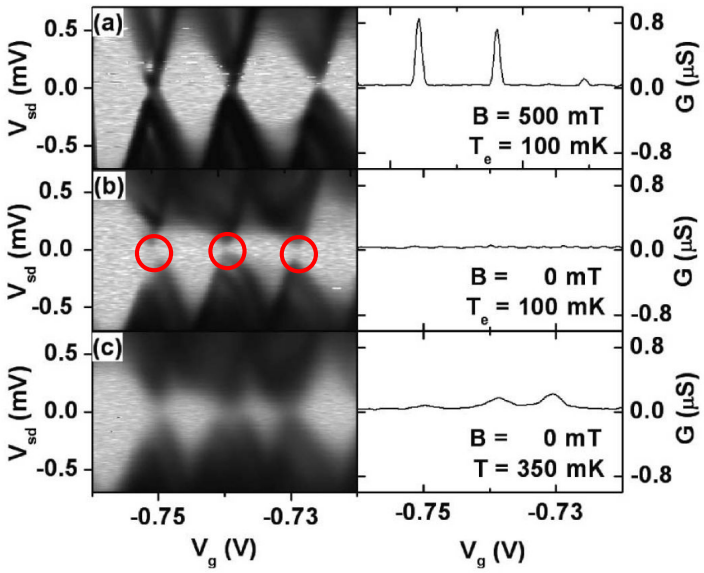

Figure 3.8: Differential conductance measured for a vibrating suspended quantum dot in an experiment by Weig et al. The regions marked in red show a significant current suppression at the charge degeneracy points, consistent with our predictions for the Franck-Condon blockade. The exact origin of the lifting of the blockade by a magnetic field is not fully understood to date. *This figure is taken from Reference [107].*

general, with rather limited microscopic input, making our results potentially applicable far beyond the particular realization of avalanche-type transport considered in the numerical simulations.

We finally remark that an experimental verification of this new transport regime depends on designing a single-molecule device with strong electron-phonon coupling and weak direct vibrational relaxation. Strong electron-phonon coupling is even realized in simple diatomic molecules such as F_2 and Kr_2 for which we estimate $\lambda \simeq 4.4$ and $\lambda \simeq 5.4$ [108], and very likely in a plethora of larger molecules. In addition, vibrational relaxation times as large as 10ns have been observed in recent experiments [44]. For these relaxation times, the regime discussed in this chapter is reached for currents large compared to 10pA.[6] Alternatively, the effects predicted here may be relevant in artificial nano-electromechanical devices. Indeed, the current suppression in the FC blockade may have recently been observed in such systems [107], see Fig. 3.8.

[6]This should be compared to currents in typical experiments ranging from nA to μA [26].